Nonlinear Optics (WiSe 2017/18)
Lecture 23: January 18, 2018

12 High-harmonic generation and attoscience

12.3 Attosecond pulses

12.3.4 Propagation effects – phase matching
12.3.5 Optimizing HHG using cycle-sculpted driver waveforms
12.3.6 RABBITT, attosecond streaking, FROG-CRAB
12.3.7 Transient XUV absorption spectroscopy
12.3.8 Attosecond ion-charge-state chronoscopy
12.3.9 Multi-purpose attoscience beamlines

Phase-matched HHG with mid-IR pulses

u_{11} mode factor

p pressure in atm

η ionization fraction

$\tilde{n}_2$ nonlinear refractive index cell. per atm

N_a number density of atoms per atm

0 for loose-focusing geometry

$$\Delta k \approx \underbrace{q\frac{u_{11}^2\lambda_L}{4\pi a^2}}_{\text{waveguide}} - \underbrace{qp(1-\eta)\frac{2\pi}{\lambda_L}(\Delta\delta + \tilde{n}_2 I)}_{\text{neutral atoms}} + \underbrace{qp\eta N_a r_e \lambda_L}_{\text{free electrons}}$$

q harmonic order

a inner wave-guide radius

$\Delta\delta = n_{gas}(\lambda_L) - n_{gas}(\lambda_L/q)$ at 1atm

r_e classical electron radius

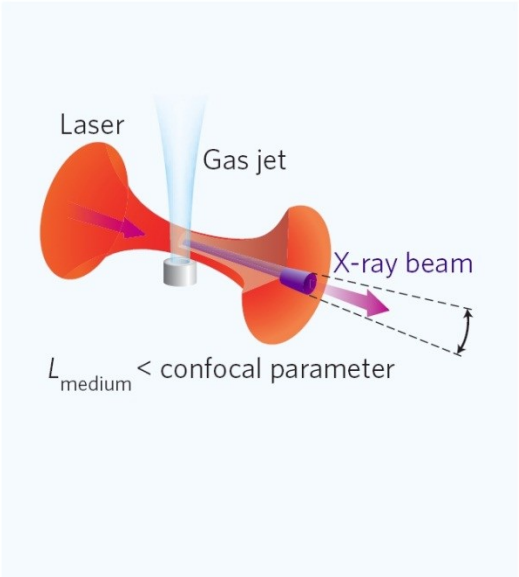

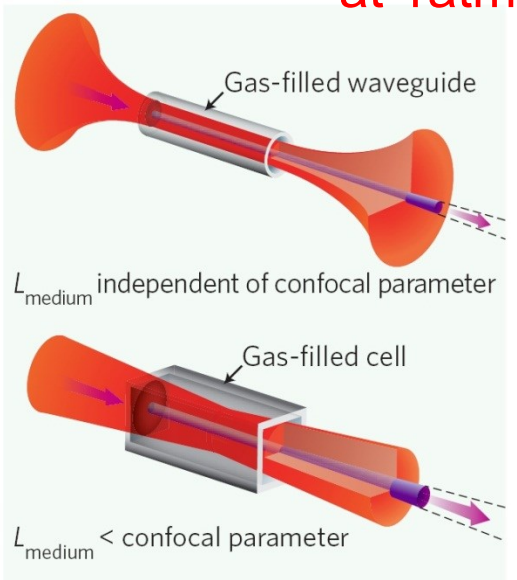

T. Popmintchev *et al.*,
PNAS **106**, 10516 (2009)
Nature Photonics **4**, 822 (2010)

E. J. Takahashi *et al.*,
PRL **101**, 253901 (2008)
PRA **66**, 021802 (2002)
IEEE JSTQE **10**, 1315 (2004)

Phase-matched HHG versus driver wavelength

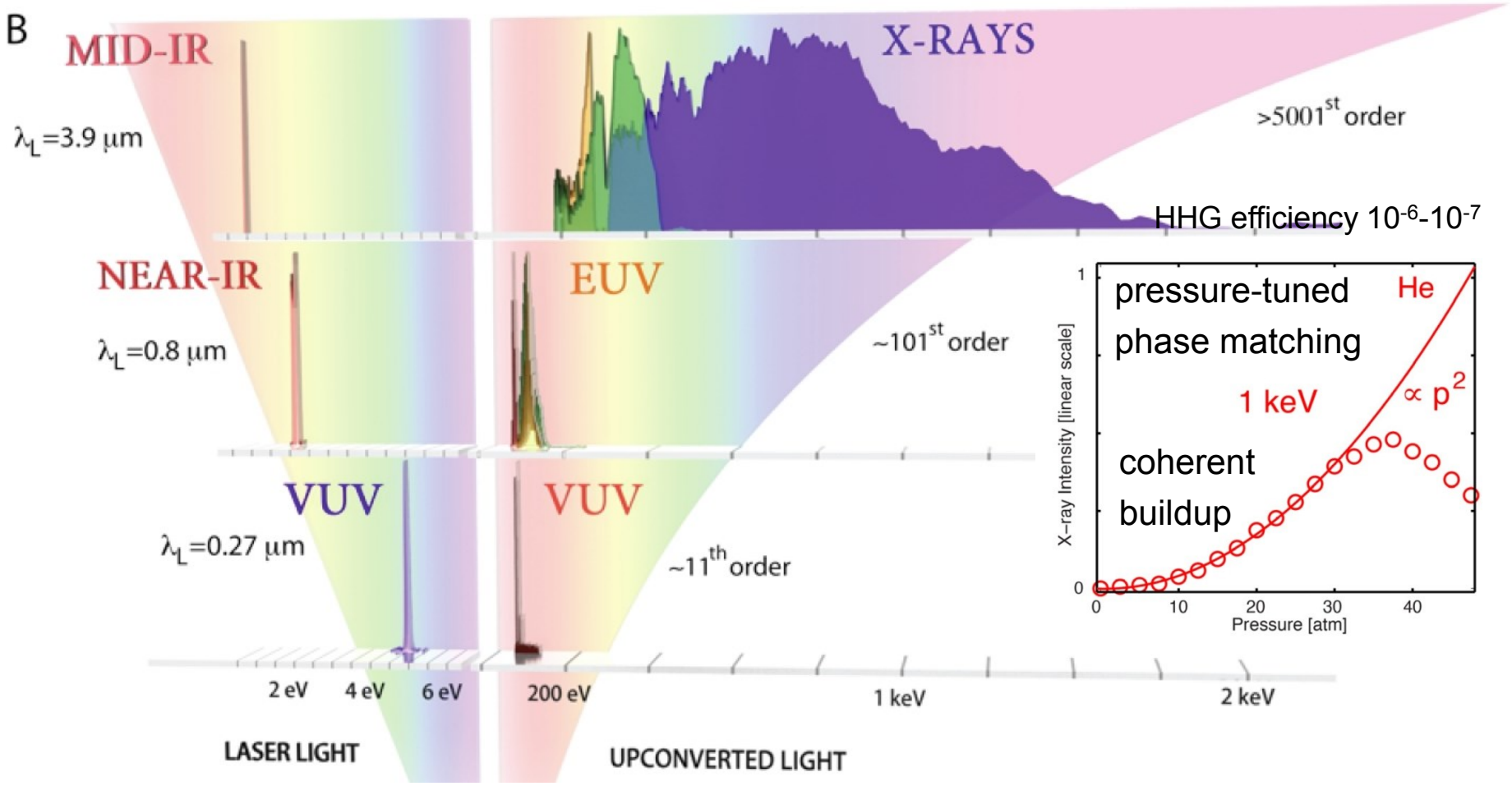

T. Popmintchev *et al.*, Science **336**, 1287 (2012)

HHG phase-matching cutoffs

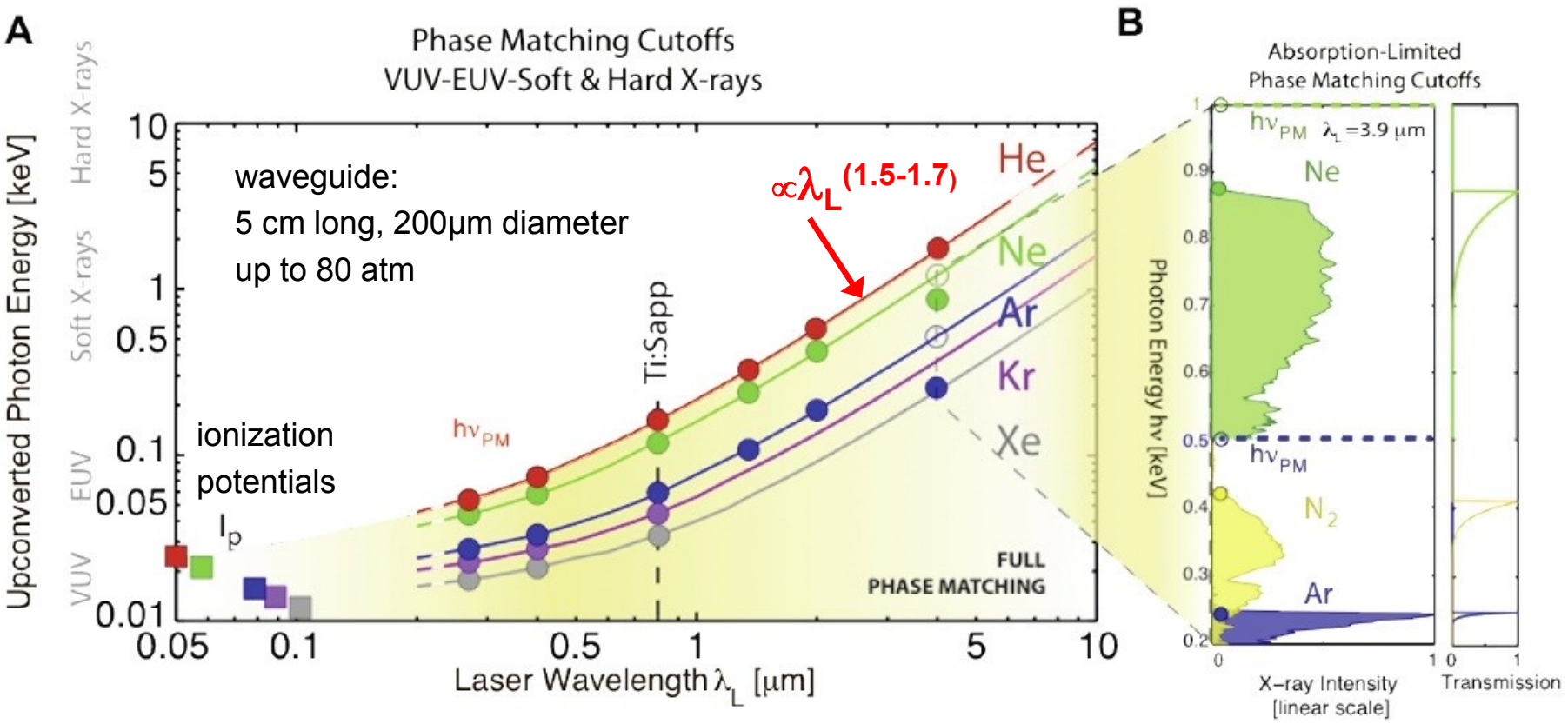

N_2: highest photon energies from molecules
→ dynamic tomographic imaging

observed cutoff for Ar and Ne below predicted cutoff (open circles) due to inner-shell absorption

T. Popmintchev *et al.*, Science **336**, 1287 (2012)

12.3.5 "Perfect wave" synthesis for HHG

synthesized from **800nm + 400nm + 267nm + 200nm + 1600nm**

ω + 2ω + 3ω + 4ω + 0.5 ω

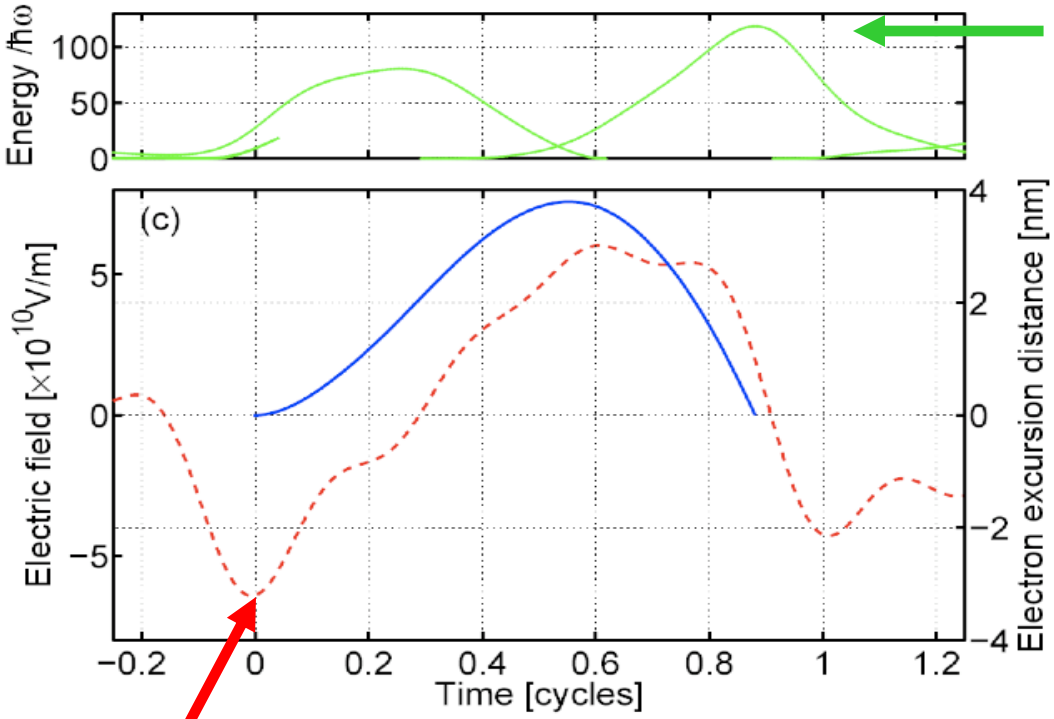

max. recollision energy

waveform	cutoff energy
sinusoidal	~ $3.17U_P$
synthesized	~ $9U_P$

high field here increases ionization probability

L. E. Chipperfield *et al.*, Phys. Rev. Lett. **102**, 063003 (2009)
C. Jin *et al.*, Nature Commun. **5**:4003 (2014)

2-photon-above-threshold-ionization (ATI) autocorr.

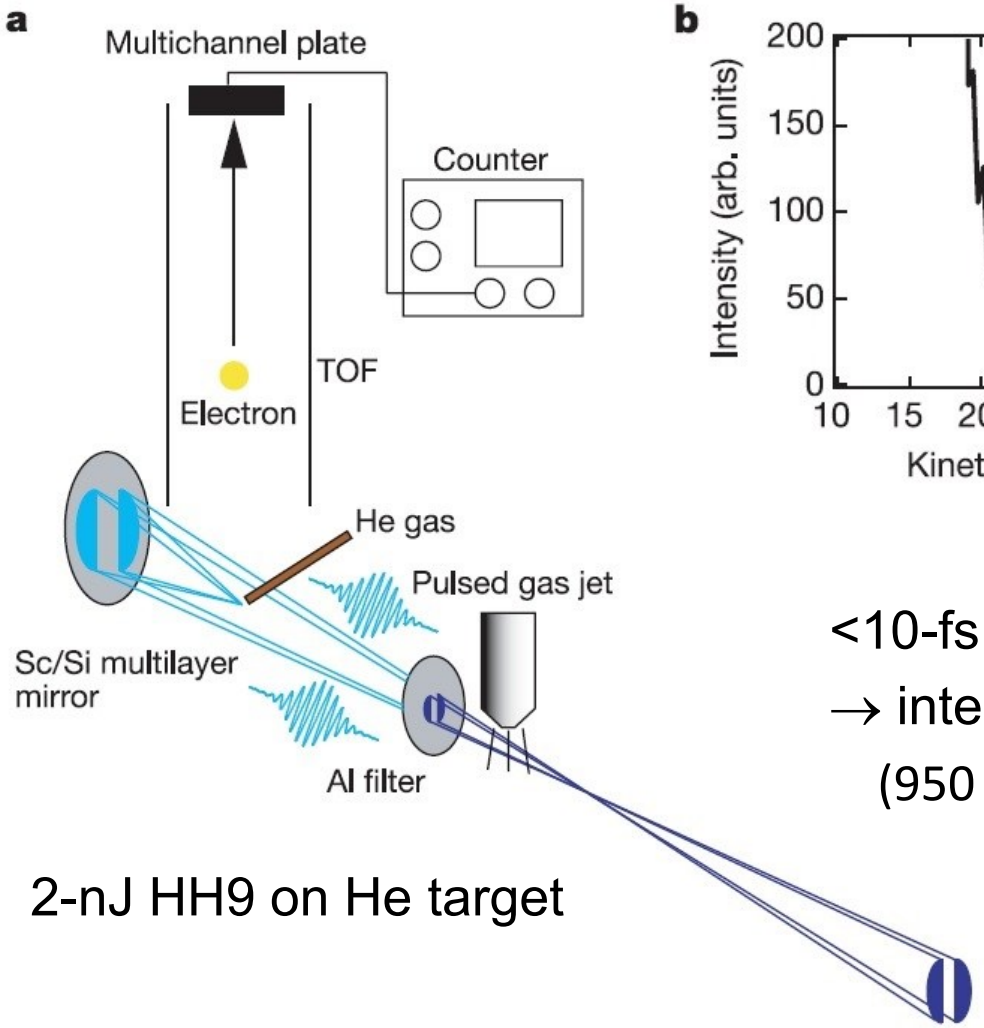

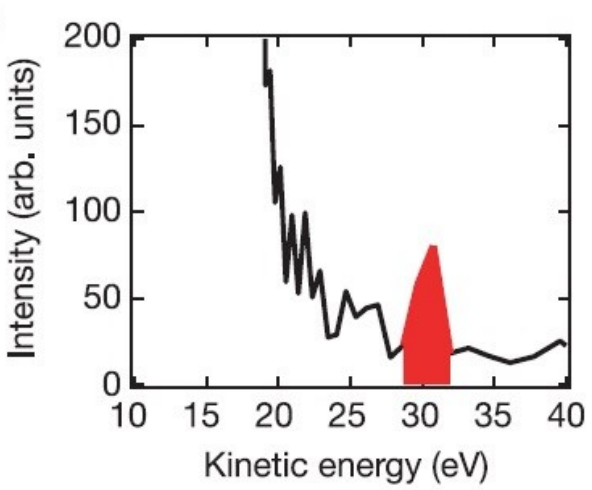

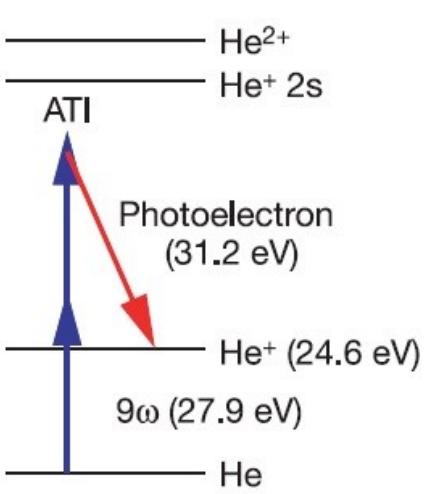

<10-fs SHG-pulses from Ti:sa (1.55 eV)

→ intense isolated 9th harmonic pulses

(950 as and 1.3 fs duration)

2-nJ HH9 on He target

T. Sekikawa *et al.*, Nature **432**, 605 (2004)

2-photon-ATI FROG

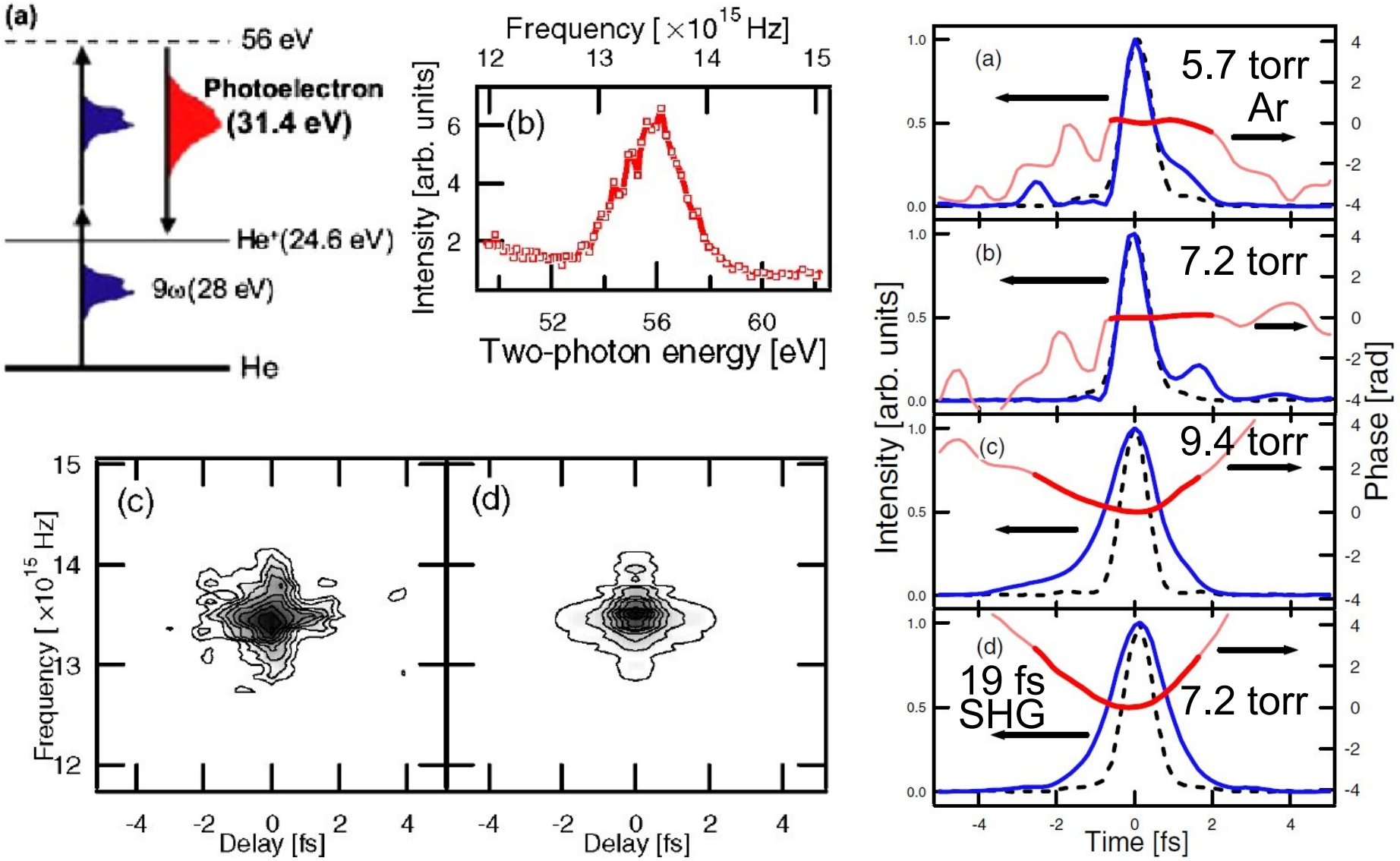

A. Kosuge *et al.*, Phys. Rev. Lett. **97**, 263901 (2006)

AC traces from side peak of N^+ ion signals

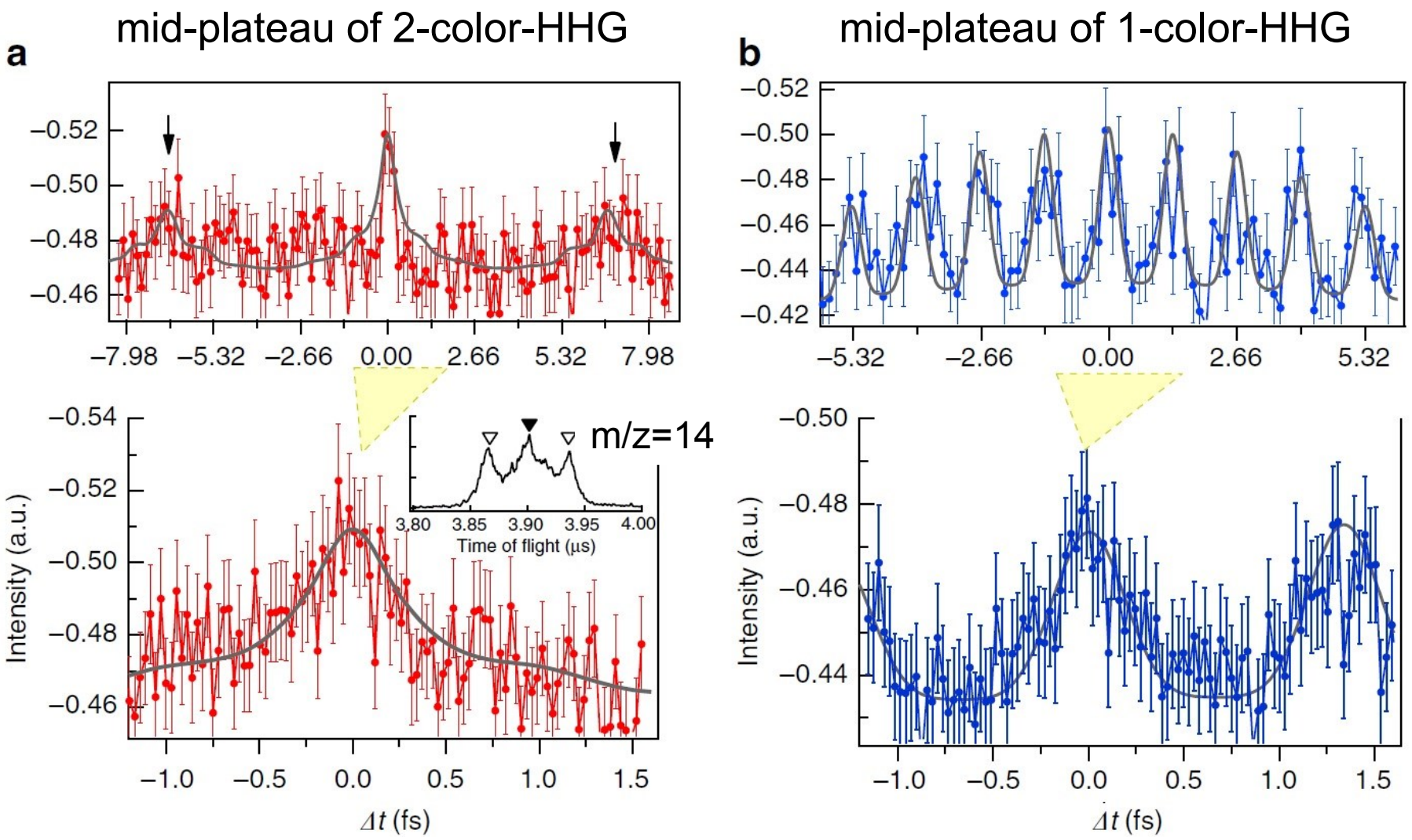

E. J. Takahashi *et al.*, Nature Commun. **4**:2691 (2013)

AC traces from side peak of N^+ ion signals

higher repetition rates → improved SNR

cutoff of 2-color-HHG

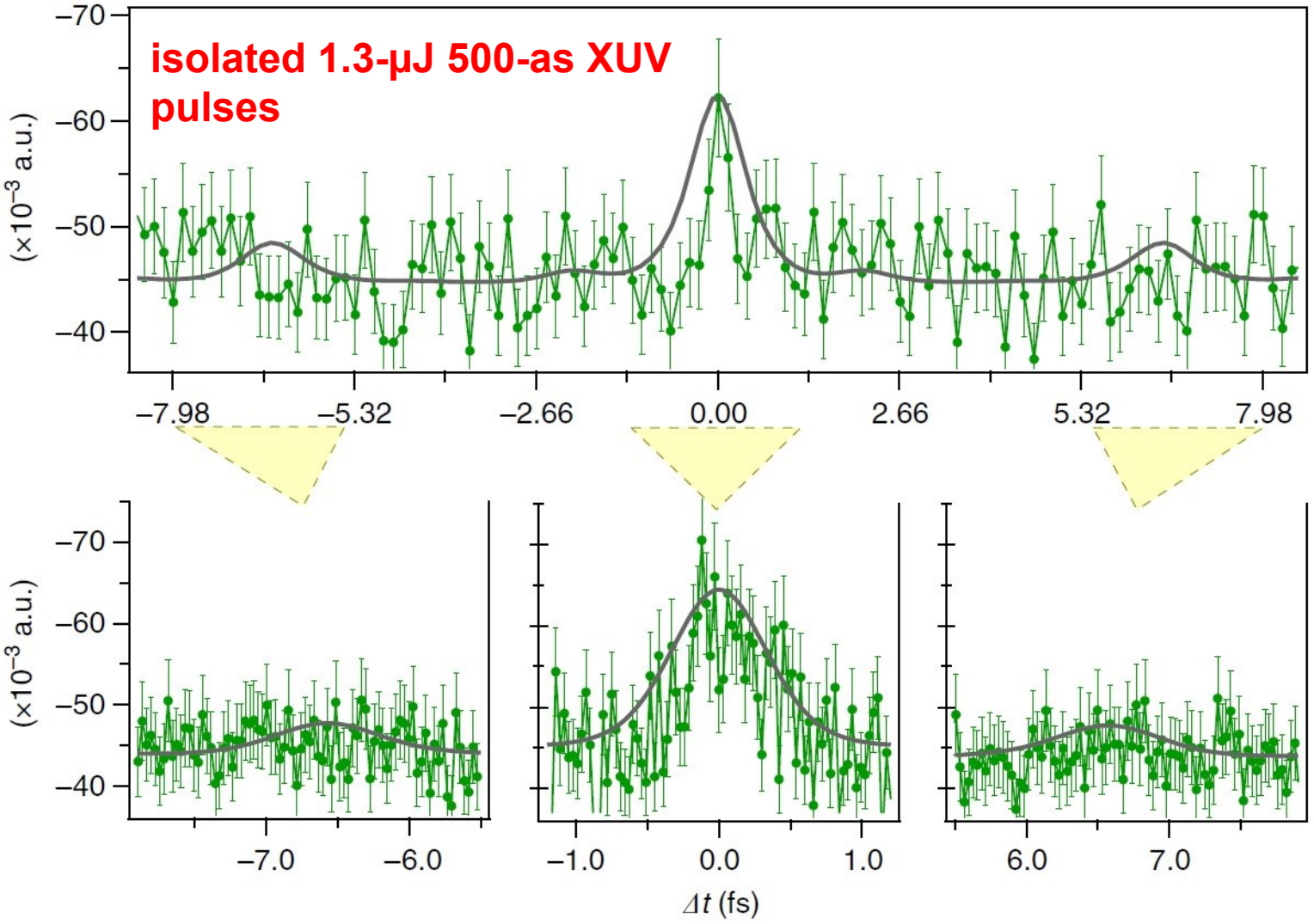

E. J. Takahashi *et al.*, Nature Commun. **4**:2691 (2013)

12.3.6 RABBITT

Reconstruction of Attosecond Beating By Interference of Two-photon Transitions (RABBITT)

V. Véniard et al., Phys. Rev. A **54**, 721 (1996)

P. M. Paul et al., Science **292**, 1689 (2001)

Y. Mairesse et al., Phys. Rev. Lett. **94**, 173903 (2005)

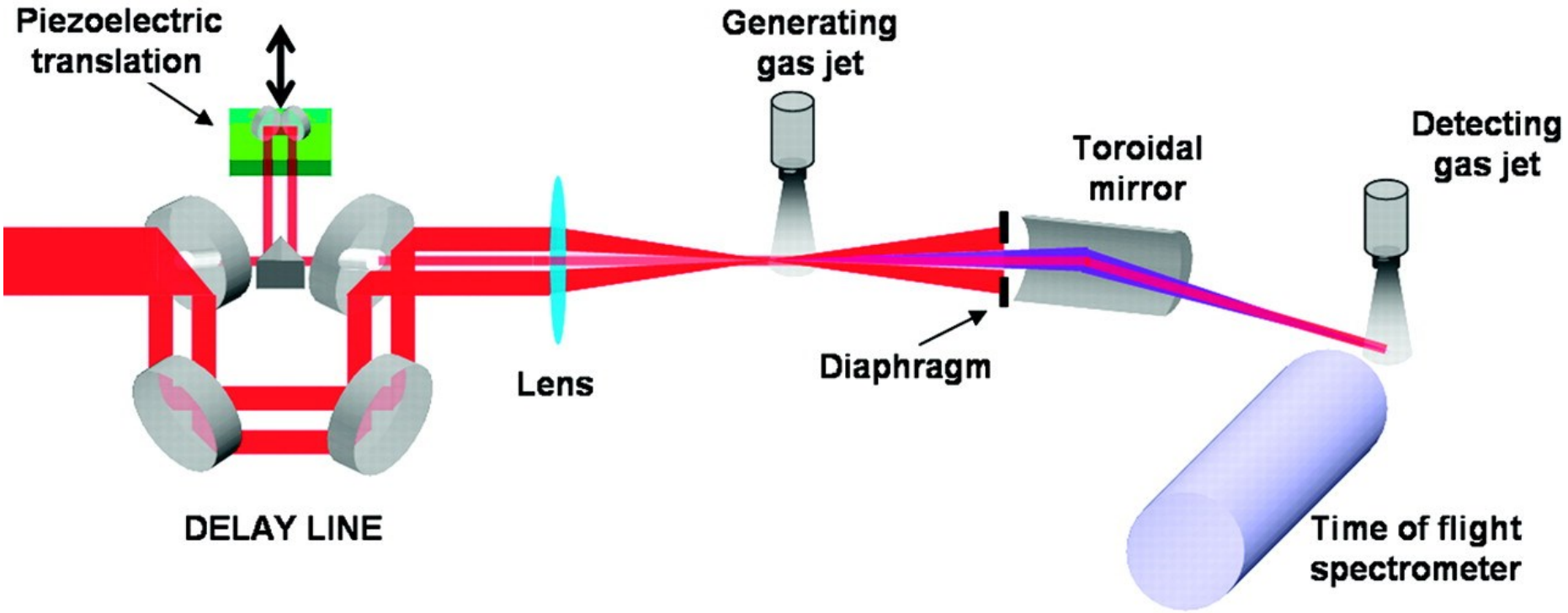

dressing intensities: typically a few 10^{11} W/cm^2

12.3.6 RABBITT

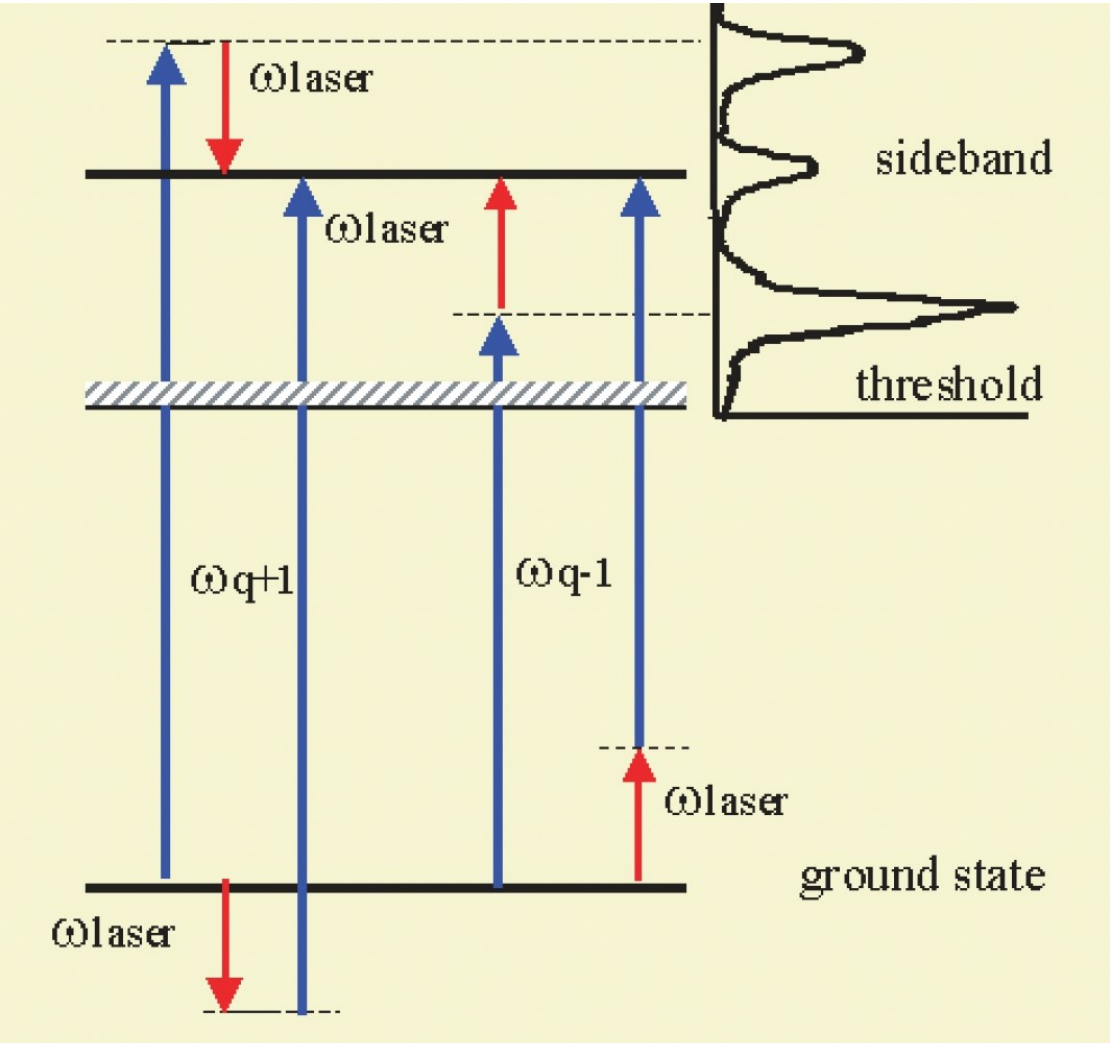

$$I_q(\Delta t) \propto \cos(2\omega_{\text{laser}}\Delta t + \varphi_{q-1} - \varphi_{q+1} + \varphi_{\text{atomic}}). \qquad (12.18)$$

electron-momentum dependent atomic phase, from dipole matrix element $\vec{d}(\vec{k})$

12.3.6 RABBITT

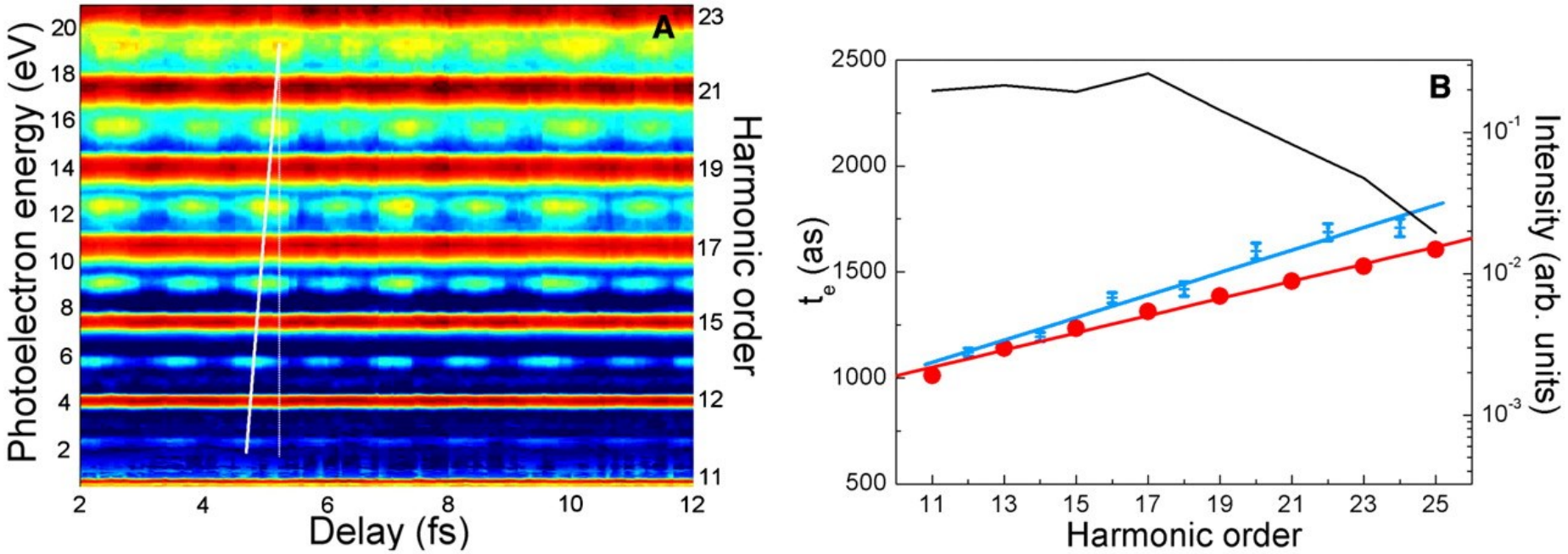

Figure 12.22: RABBITT measurement of the emission time of harmonics in Ar driven by a Ti:sapphire pulse with peak intensity $I_{IR} = 1.2 \times 10^{14}\,W/cm^2$. (A) Photoelectron spectrum versus XUV-NIR delay. The spectra are normalized and displayed on a nonlinear color scale. The thick white line is a guide to the eye indicating the sideband maxima; the thin line indicates a fixed delay. (B) Extracted harmonic emission time: measurements (blue crosses with error bars) and theoretical predictions by single-atom response (red dots). Linear fits (blue and red curves) yields the emission time shift between consecutive harmonics as $t_e^{exp} = (106 \pm 8)$ as and $t_e^{theo} = (81 \pm 3)$ as. The black line shows the measured harmonic intensity. [55]

Y. Mairesse *et al.*, Phys. Rev. Lett. **94**, 173903 (2005)

12.3.6 Attosecond streaking

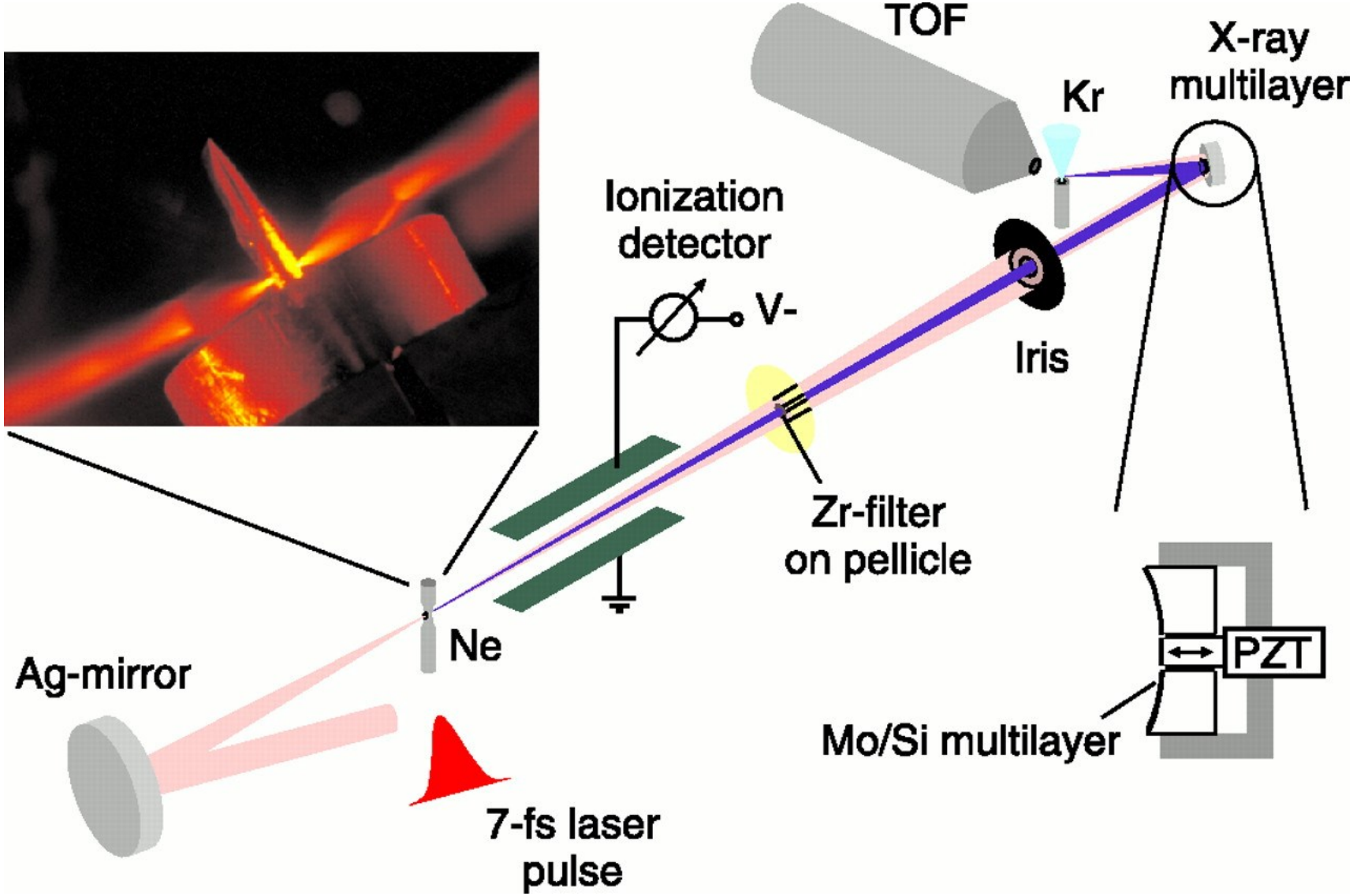

M. Drescher *et al.*, Science **291**, 1923 (2001)

Attosecond streaking geometries

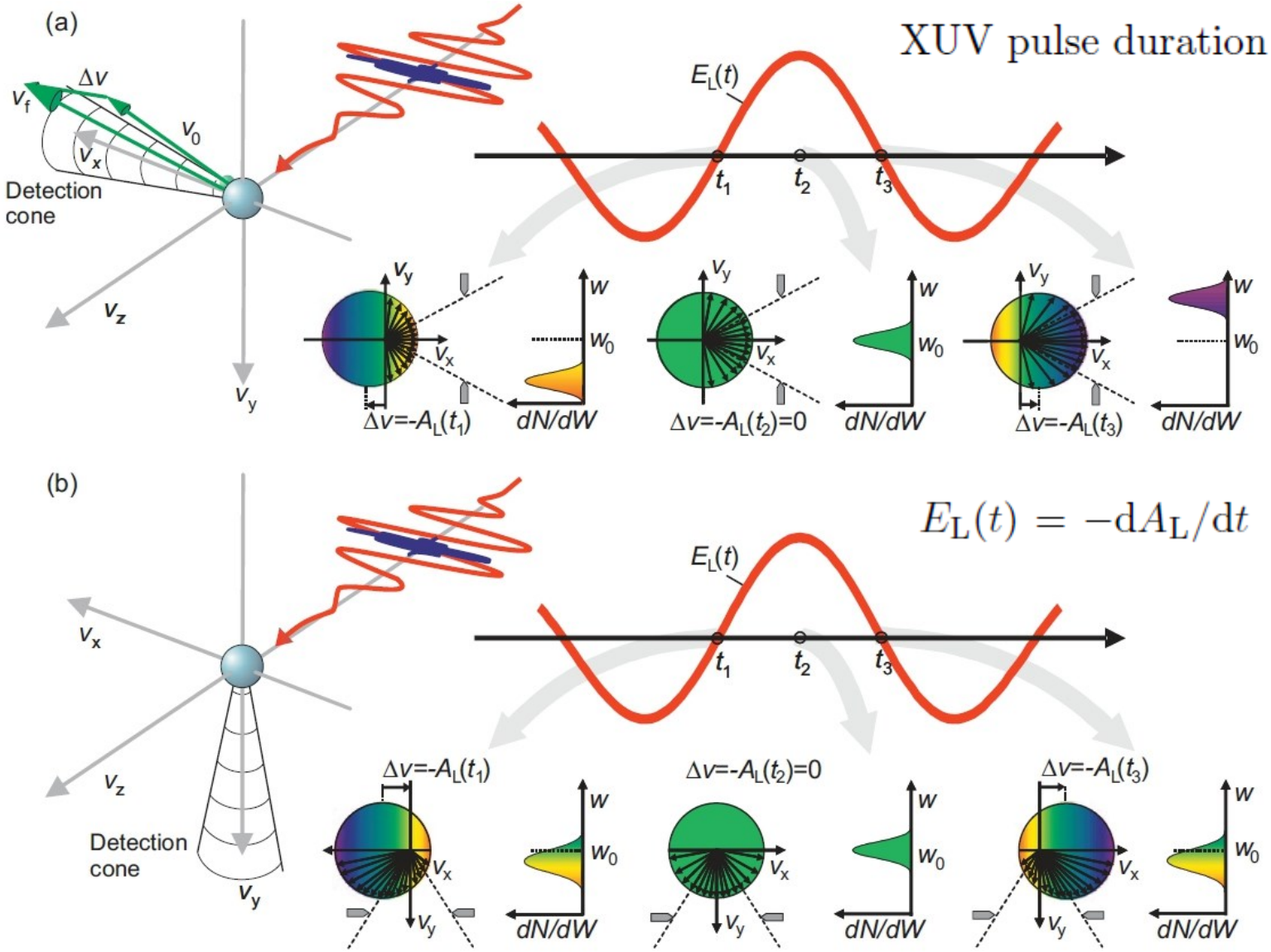

F. Krausz and M. Ivanov, Rev. Mod. Phys. **81**, 163 (2009)

Attosecond streaking geometries

pendicular TOF detection geometry, as sketched in Fig. 12.24. The influence of the detection geometry can be understood by a semi-classical treatment integrating the classical equations of motion of an electron inside a laser field (for details, see [56, 57, 2]). Within the slowly-varying envelope approximation (SVEA, $\mathrm{d}\tilde{E}_\mathrm{L}/\mathrm{d}t \ll \omega_\mathrm{L}\tilde{E}_\mathrm{L}$), one obtains for the final energy of the electrons

$$W_f = W_0 + 2U_p(t_d)\cos 2\theta \sin^2 \omega_\mathrm{L} t_d \pm \alpha_\mathrm{L}\sqrt{8W_0U_p(t_d)}\cos\theta \sin \omega_\mathrm{L} t_d\,. \quad (12.19)$$

$W_0 = \hbar\omega_\mathrm{XUV} - W_b$ is the initial kinetic energy of the photoelectron, W_b the atomic binding energy, θ is the angle between the final momentum of the electron and the laser electric-field vector, and t_d the the XUV-NIR delay. The prefactor of the third term

$$\alpha_\mathrm{L} = \{1 - (2U_p(t_d)/W_0)\sin^2\theta \sin^2 \omega_\mathrm{L} t_d\}^{1/2} \quad (12.20)$$

is close to unity if U_p is much smaller than W_0.

In the parallel detection geometry ($\theta = 0$, Fig. 12.24(a)) and assuming $U_p \ll W_0$, the second term in (12.19) can be neglected and the main effect is a

M. Drescher *et al.*, Science **291**, 1923 (2001)
J. Itatani *et al.*, Phys. Rev. Lett. **88**, 173903 (2002)

Attosecond streaking geometries

shift up and down of the electron energy relative to the field-free value. This geometry offers the largest streaking, and permits to use large TOF collection angles since $\cos\theta$ does not vary much up to $\pm 30°$. A drawback is that the energy shift depends on W_0, which can become a problem if the bandwidth of the wavepacket becomes comparable to its mean energy [2]. This geometry is used in most experiments.

In the perpendicular detection geometry ($\theta = 90°$, Fig. 12.24(b)), the third term vanishes and Eq. (12.19) can be rewritten as $W_f = W_0 - U_p(t_d) + U_p(t_d)\cos 2\omega_L t_d$. When the delay t_d is scanned, the photoelectron peak experiences a ponderomotive down-shift and oscillates between 0 and $2U_p$ with a period of $T/2$ corresponding to an oscillating spectral broadening. The perpendicular detection geometry was actually used in the first demonstrations of attosecond streaking [57, 18], as shown in Fig. 12.25.

M. Drescher *et al.*, Science **291**, 1923 (2001)
J. Itatani *et al.*, Phys. Rev. Lett. **88**, 173903 (2002)

Attosecond streaking: perpendicular geometry

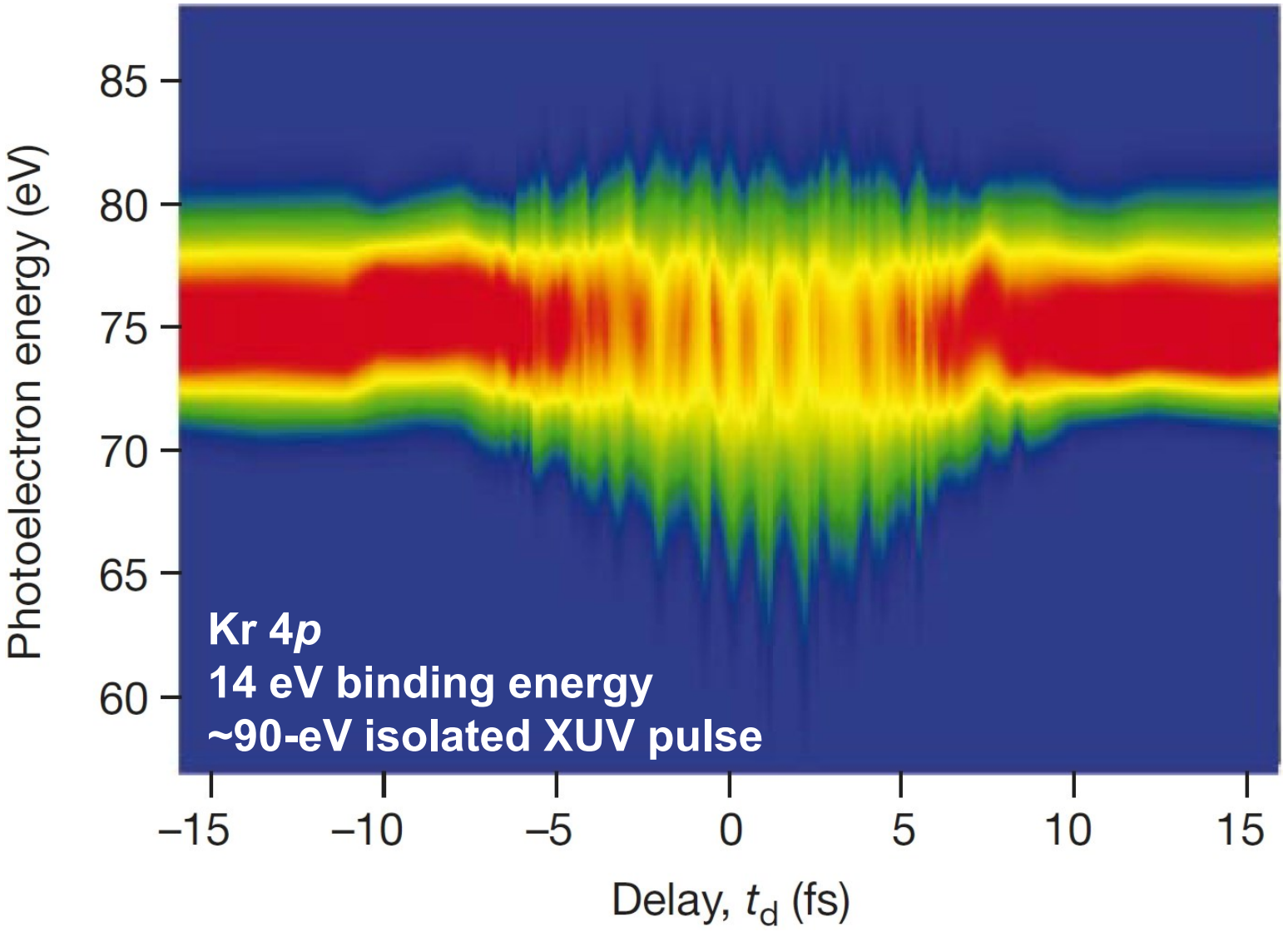

M. Hentschel *et al.*, Nature **414**, 509 (2001)

Lightwave oscilloscope: parallel geometry

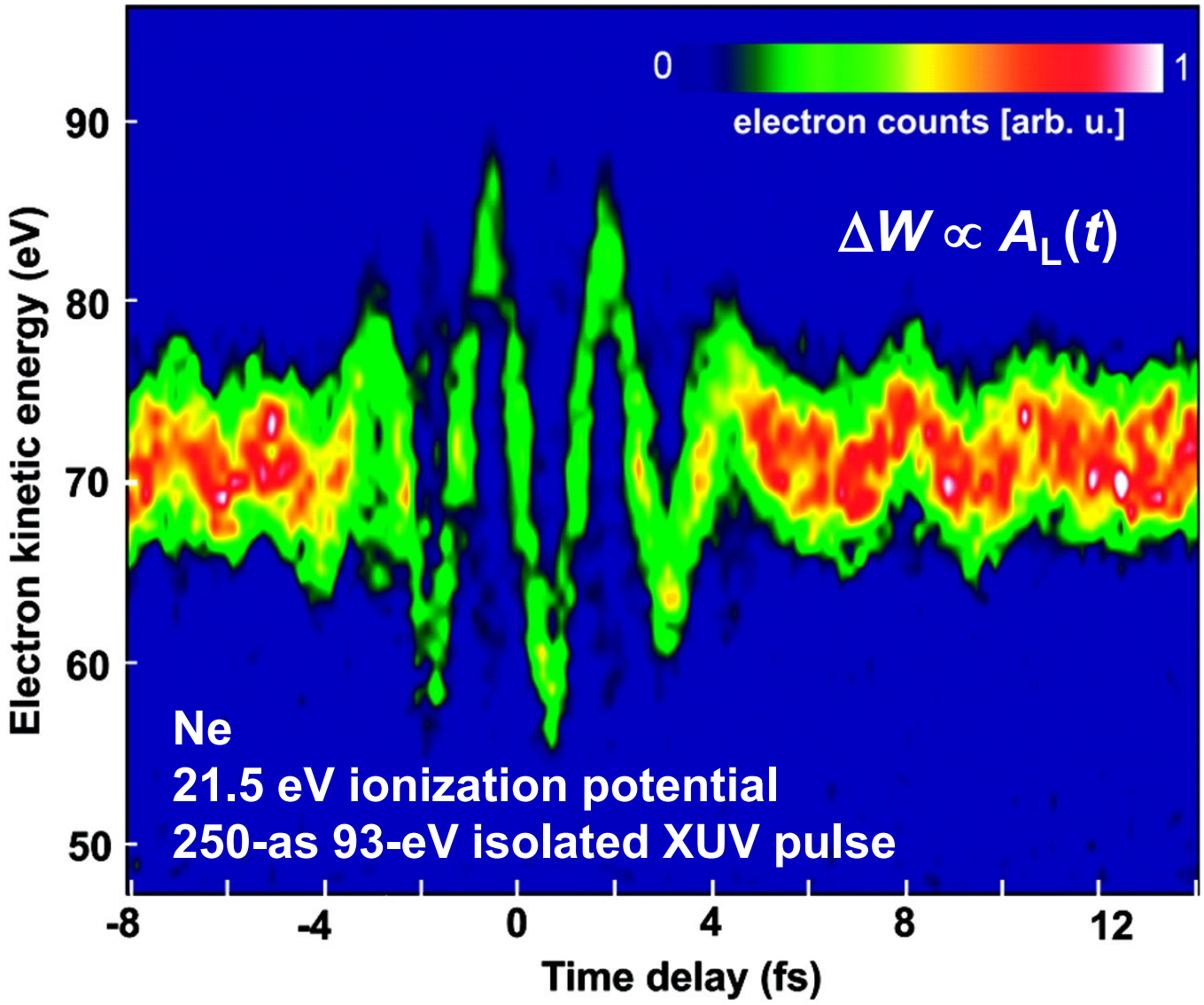

E. Goulielmakis *et al.*, Science **320**, 1614 (2008)

Lightwave oscilloscope: parallel geometry

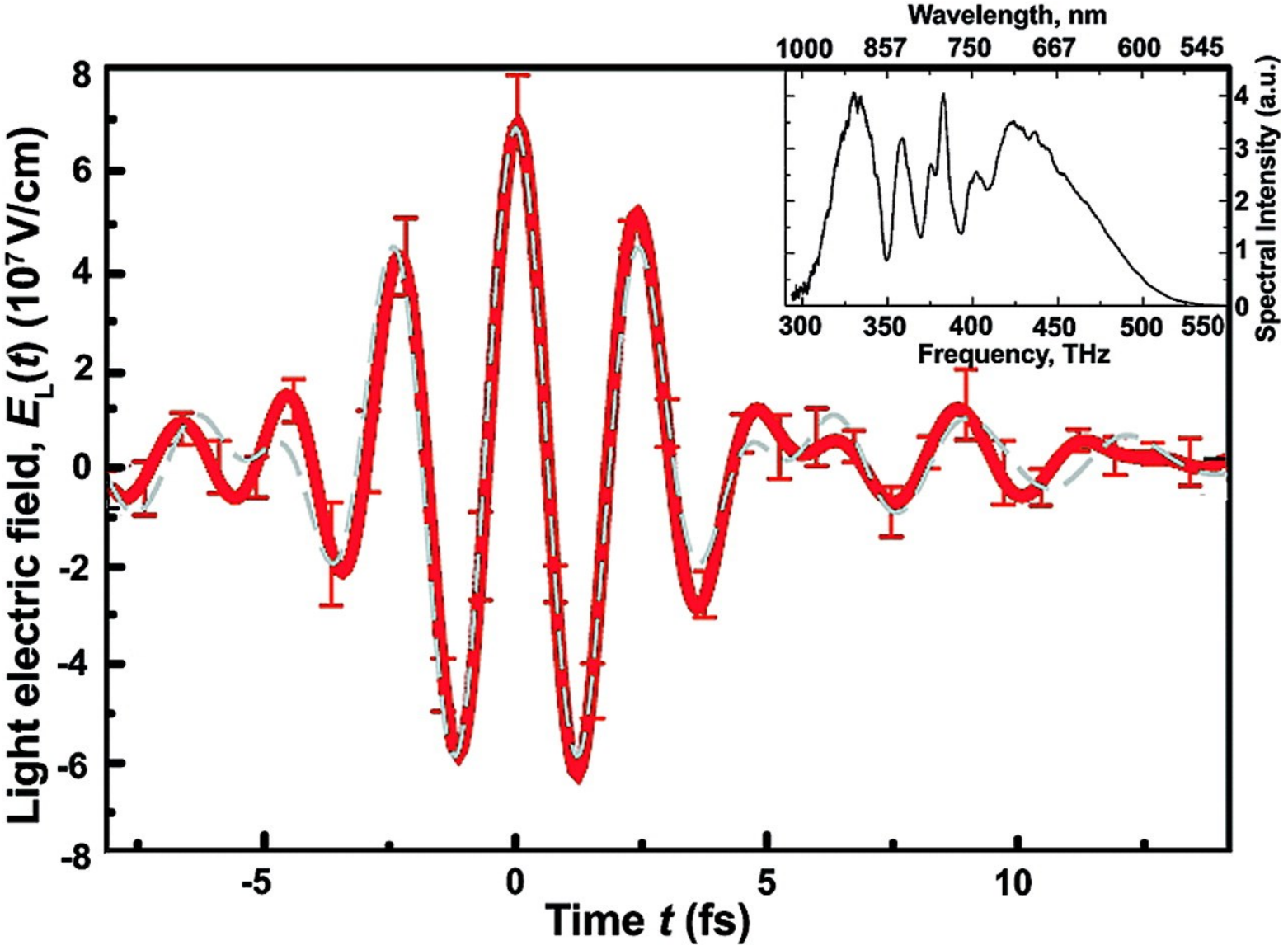

E. Goulielmakis *et al.*, Science **320**, 1614 (2008)

Attosecond streak camera

set of tomographic projections

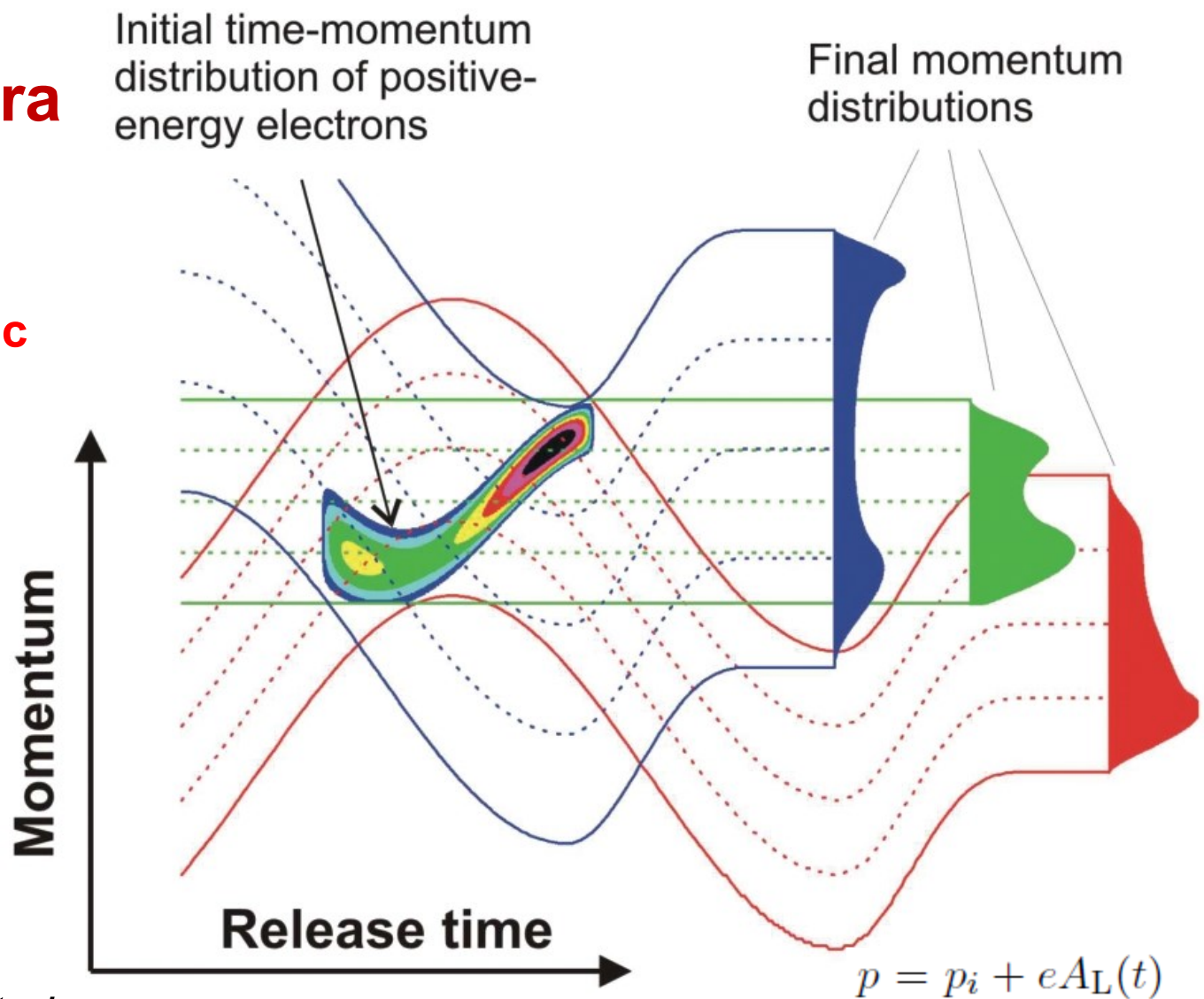

$$p = p_i + eA_{\mathrm{L}}(t)$$

R. Kienberger *et al.*,
Nature 427, 817 (2004)

$$\sigma(p) = \int_{-\infty}^{+\infty} \mathrm{d}t\, n_e(p - eA_{\mathrm{L}}(t), t)$$

Attosecond streak camera

mapping time to momentum

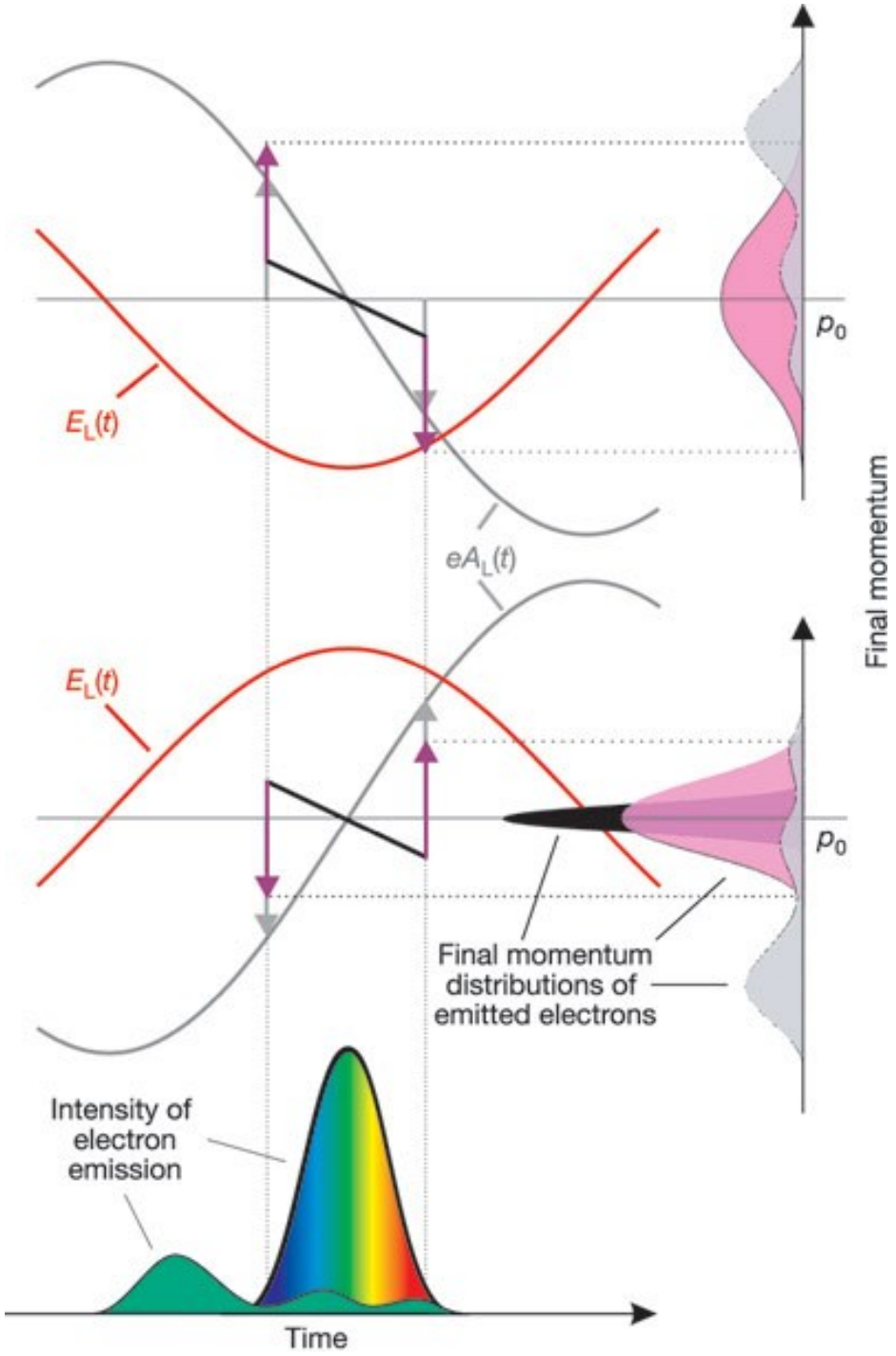

R. Kienberger *et al.*, Nature 427, 817 (2004)

FROG-CRAB

Frequency-Resolved Optical Gating for Complete Retrieval of Attosecond Bursts
Y. Mairesse and F. Quéré, Phys. Rev. A 71, 011401 (2005)

In [69, 70], the deep connection between RABBITT and attosecond streaking was revealed and unified to the more general FROG-CRAB technique. Within the framework of the strong-field approximation (SFA) [7, 3], the transition amplitude to the final continuum state $|\mathbf{v}\rangle$ of the electron with momentum $\mathbf{v}$ can be expressed as [70]

$$a(\mathbf{v}, \Delta t) = -i \int_{-\infty}^{+\infty} \mathrm{d}t \, e^{i\phi(t)} \mathbf{d}_{\mathbf{p}(t)} \mathbf{E}_{\mathrm{XUV}}(t - \Delta t) e^{i(\mathbf{v}^2/2 + I_p)t} , \quad (12.22)$$

$$\phi(t) = -\int_{t}^{+\infty} \mathrm{d}t' [\mathbf{v}\mathbf{A}_{\mathrm{L}}(t') + \mathbf{A}_{\mathrm{L}}^2(t')/2] . \quad (12.23)$$

Here, $\mathbf{E}_{\mathrm{XUV}}(t)$ is the XUV electric field, $\mathbf{A}_{\mathrm{L}}(t)$ the laser vector potential of the dressing pulse, $\mathbf{p}(t) = \mathbf{p} + \mathbf{A}(t)$, $\mathbf{d}_{\mathbf{p}}$ the dipole matrix element from the ground state to a continuum state $|\mathbf{p}\rangle$, I_p the atom's ionization potential. $\phi(t)$ represents the quantum phase acquired by the electron in the continuum due to its interaction with the laser field. The measured spectrograms are then given by the square modulus of the transition amplitude, i.e., $S(\mathbf{v}, \Delta t) = |a(\mathbf{v}, \Delta t)|^2$.

FROG-CRAB

Frequency-Resolved Optical Gating for Complete Retrieval of Attosecond Bursts
Y. Mairesse and F. Quéré, Phys. Rev. A 71, 011401 (2005)

As shown in [69, 70], Eq. (12.23) has an intuitive interpretation: the laser electric field induces a phase modulation on the electron wavepacket during its propagation in the continuum, after being created by the XUV field. In RABBITT, for attosecond XUV pulse trains generated from multi-cycle laser fields, the weak dressing field acts as a periodic phase modulator on the electron wavepacket, thus creating the sidebands that are used to retrieve the harmonic phases. In attosecond streaking, for isolated XUV pulses generated from few-cycle laser fields, the XUV pulse is significantly shorter than then the optical period of the strong streaking laser field, thus creating the characteristic streaking spectrograms.

FROG-CRAB

Frequency-Resolved Optical Gating for Complete Retrieval of Attosecond Bursts
Y. Mairesse and F. Quéré, Phys. Rev. A 71, 011401 (2005)

The spectrograms $S(\mathbf{v}, \Delta t) = |a(\mathbf{v}, \Delta t)|^2$ given by Eq. (12.23) resemble the well-known FROG trace

$$S(\omega, \Delta t) = \left| \int_{-\infty}^{+\infty} \mathrm{d}t\, G(t) E(t - \Delta t) e^{i\omega t} \right|^2 \qquad (12.24)$$

In standard FROG, $G(t)$ represents a pure *amplitude gate*, and efficient algorithms (e.g., the generalized projections algorithms) can be used to retrieve $E(t)$ and the gate $G(t)$ from the spectrogram. Inspection of Eq. (12.23) suggests that in FROG-CRAB, $G(t) = e^{i\phi(t)}$ could be used as a pure *phase gate* for the reconstruction. However, a requirement for the applicability of generalized projections algorithms to FROG-CRAB is that there cannot be inseparable terms inside the integrand of Eq. (12.23) that depend both on momentum and time [71]. Obviously, two terms in Eq. (12.23) cause trouble: $\mathbf{d}_{\mathbf{p}(t)}$ and $\phi(t)$. The standard remedy to fix this issue is to make the *central momentum approximation* (CMA), by substituting $\mathbf{p}(t)$ with the central momentum of the

FROG-CRAB

Frequency-Resolved Optical Gating for Complete Retrieval of Attosecond Bursts
Y. Mairesse and F. Quéré, Phys. Rev. A 71, 011401 (2005)

unstreaked electrons $\mathbf{p}_0$ (and $\mathbf{v}$ by $\mathbf{v}_0$). The CMA is good as long as the bandwidth of the attosecond pulse is much smaller than the central energy of the photoelectrons. Interestingly, for recent state-of-the-art experiments [19, 20], the CMA is only barely met, the isolated 65-as pulses in [61] already violate this approximation. For such ultrabroadband XUV pulses novel retrieval algorithms, that do not employ the CMA, have been developed, e.g, *Phase Retrieval by Omega Oscillation Filtering* (PROOF) [72] and *Volkov transform generalized projections algorithm* (VTGPA) [73] .

Coming back to FROG-CRAB: as can be seen by the reconstructions shown in Figs. 12.29, 12.30, and 12.31, FROG-CRAB provides a unified framework to characterize APTs and and IAPs and even more complex fields.

PROOF: M. Chini *et al.*, Opt. Express 18, 13006 (2010)
VTGPA: P. D. Keathley *et al.*, New J. Phys. **18**, 073009 (2016)

FROG-CRAB

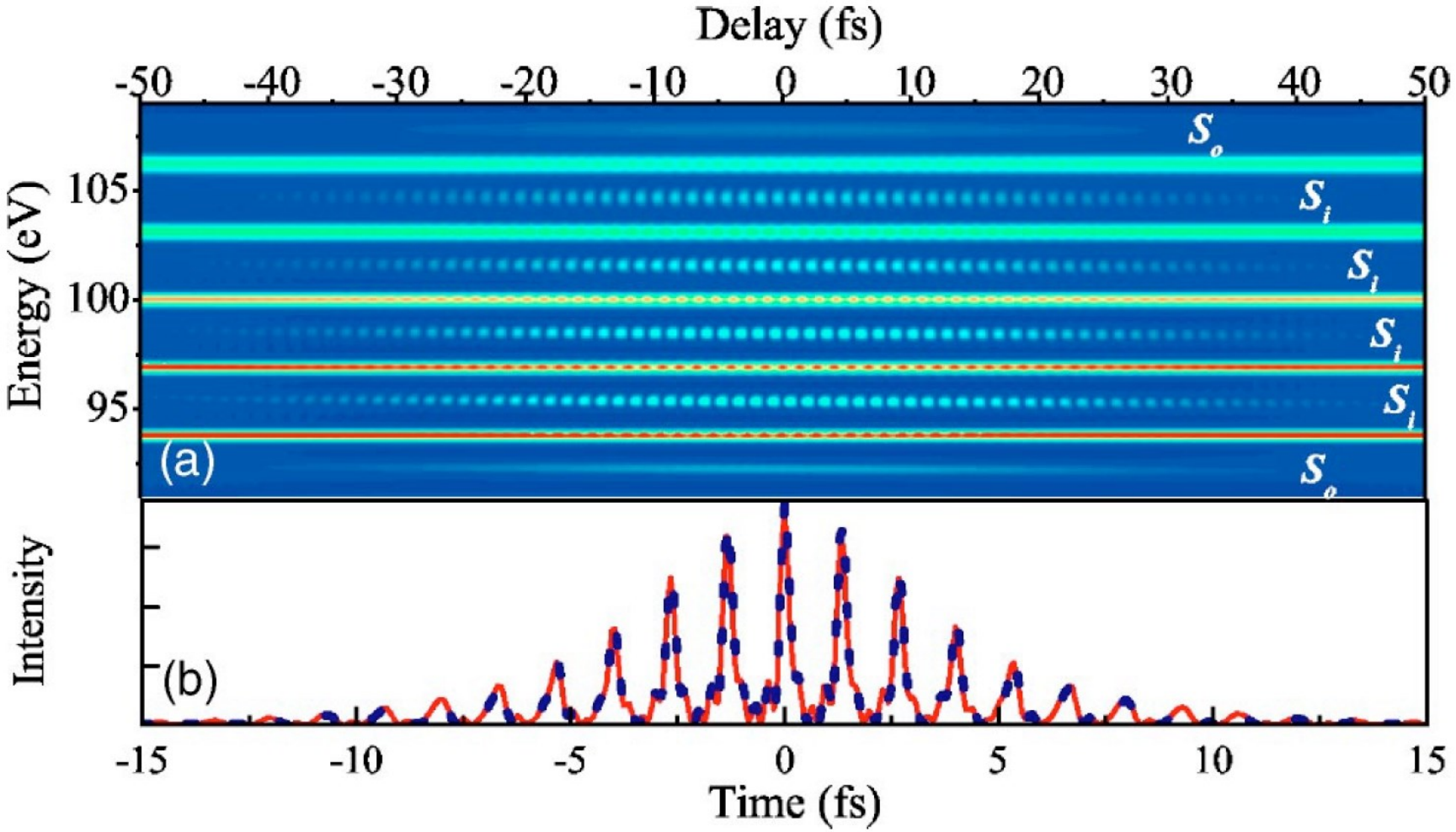

Y. Mairesse and F. Quéré, Phys. Rev. A 71, 011401 (2005)

FROG-CRAB

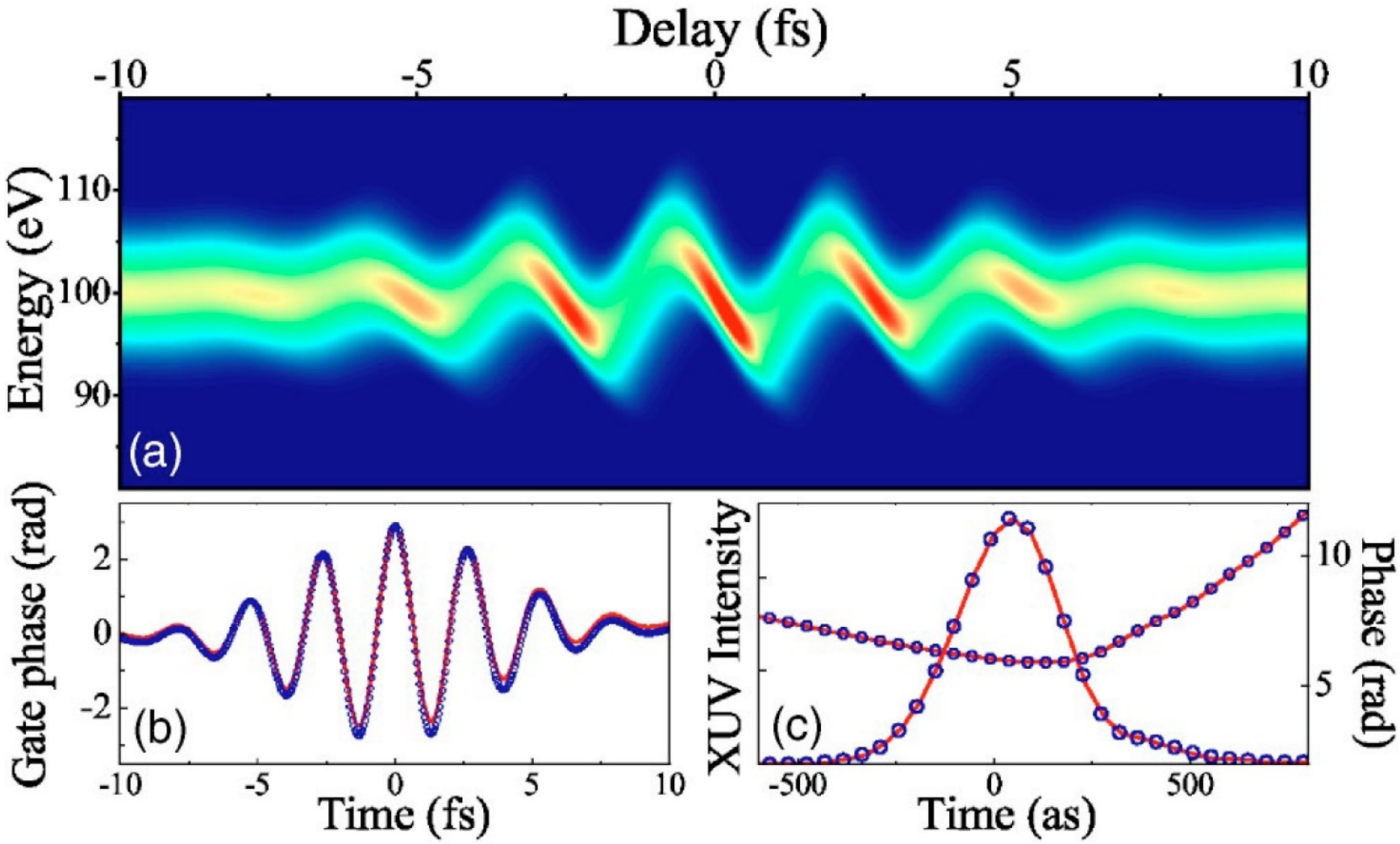

Y. Mairesse and F. Quéré, Phys. Rev. A 71, 011401 (2005)

FROG-CRAB

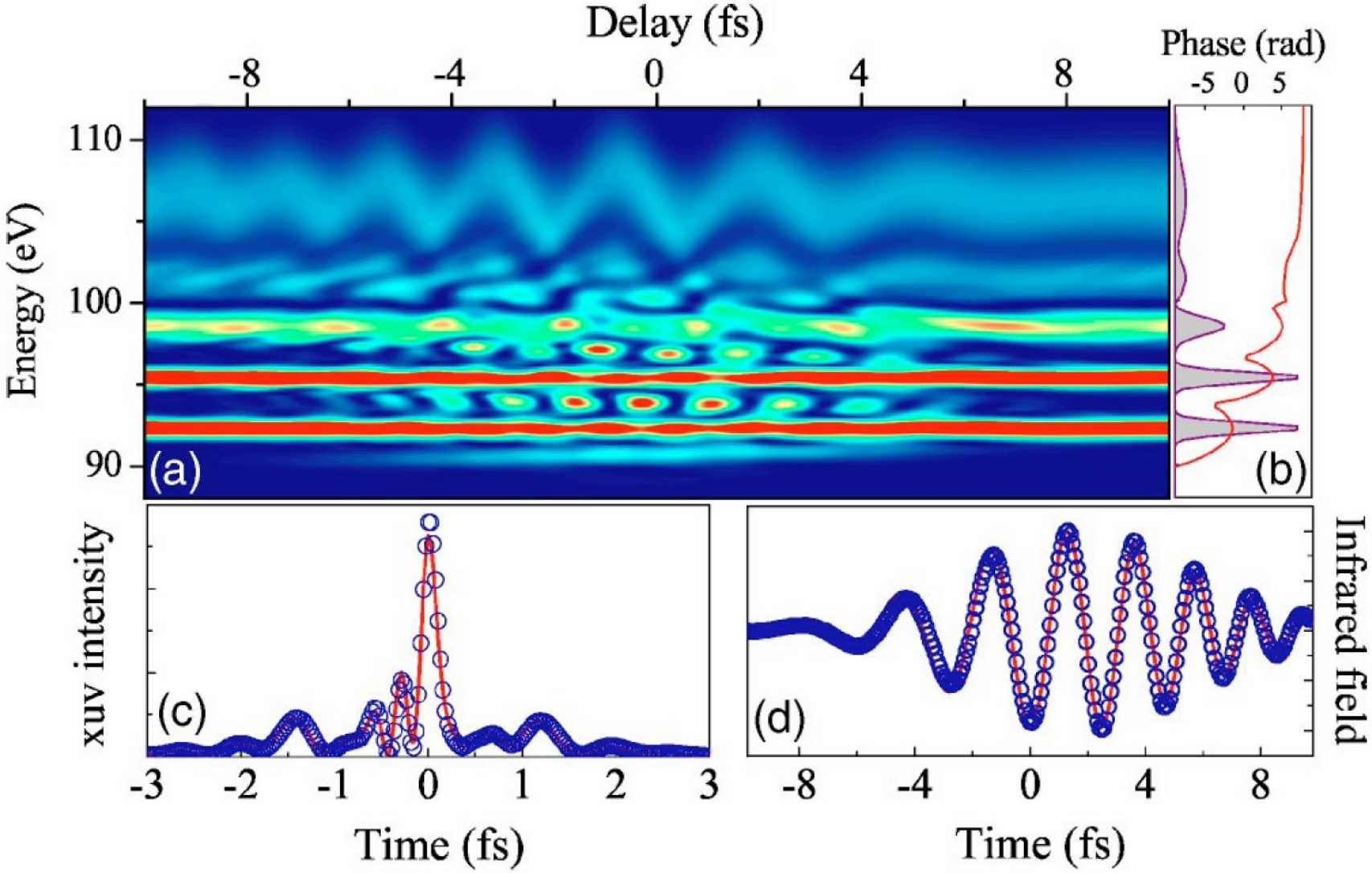

Y. Mairesse and F. Quéré, Phys. Rev. A 71, 011401 (2005)

12.3.7 Transient XUV absorption spectroscopy

changes induced by a first strong pump pulse are probed by the **transient absorption changes of an isolated attosecond XUV pulse**

real-time observation of valence electron motion in Kr:
E. Goulielmakis *et al.*, Nature **466**, 739 (2010)

observation of Autler-Townes splitting and sub-cycle AC Stark shifts in He:
M. Chini *et al.*, Sci. Rep. **3**, 1105 (2013).

laser control between symmetric Lorentzian and asymmetric Fano line shapes in He:
C. Ott *at al.*, Science **340**, 716 (2013)

observation and control of two-electron wave packets in He:
C. Ott *et al.*, Nature **516**, 374 (2014)

Show video!

12.3.8 Attosecond ion-charge-state chronoscopy

attosecond tunneling spectroscopy

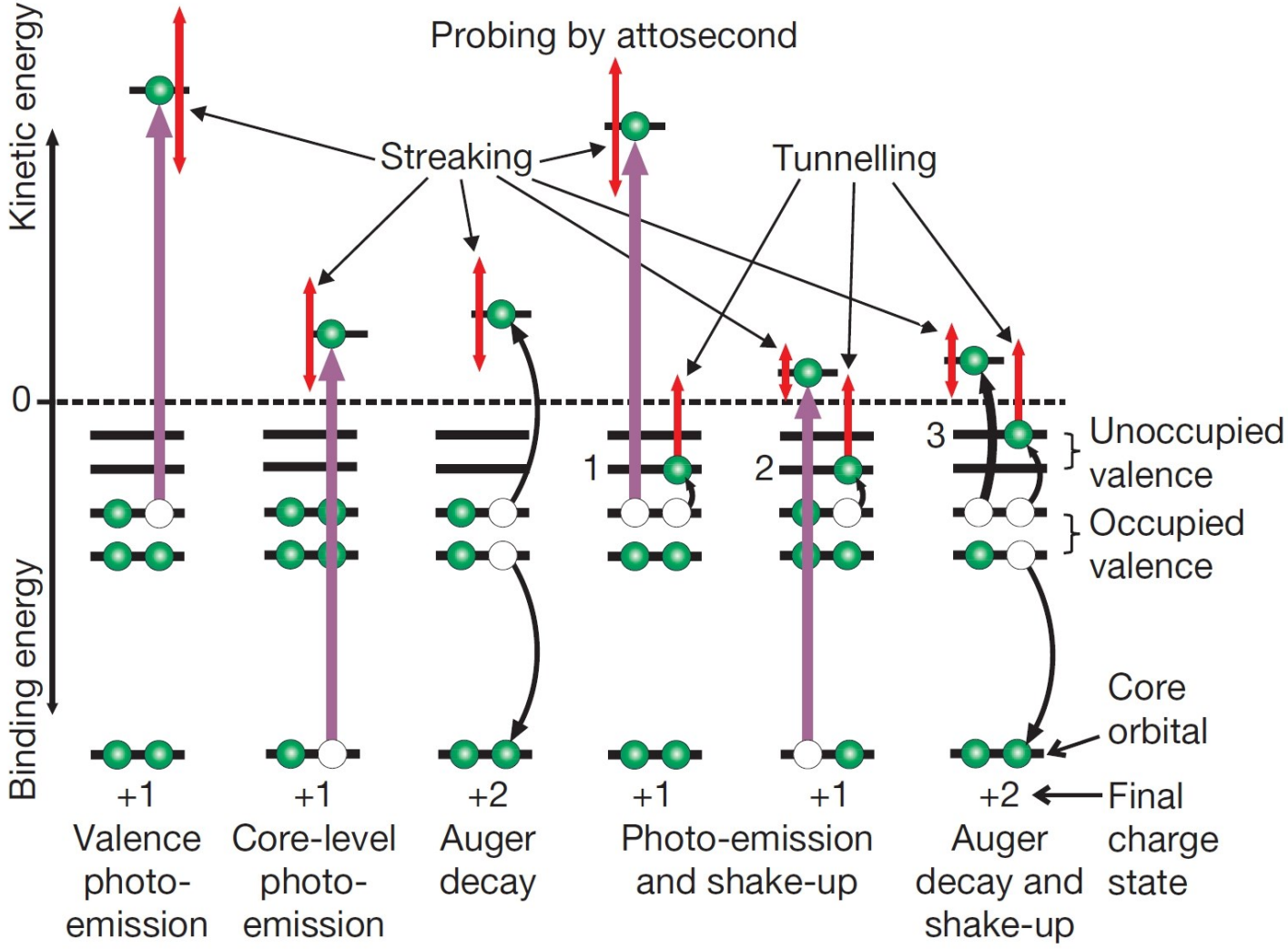

M. Uiberacker *et al.*, Nature **446**, 627 (2007)

Attosecond tunneling spectroscopy

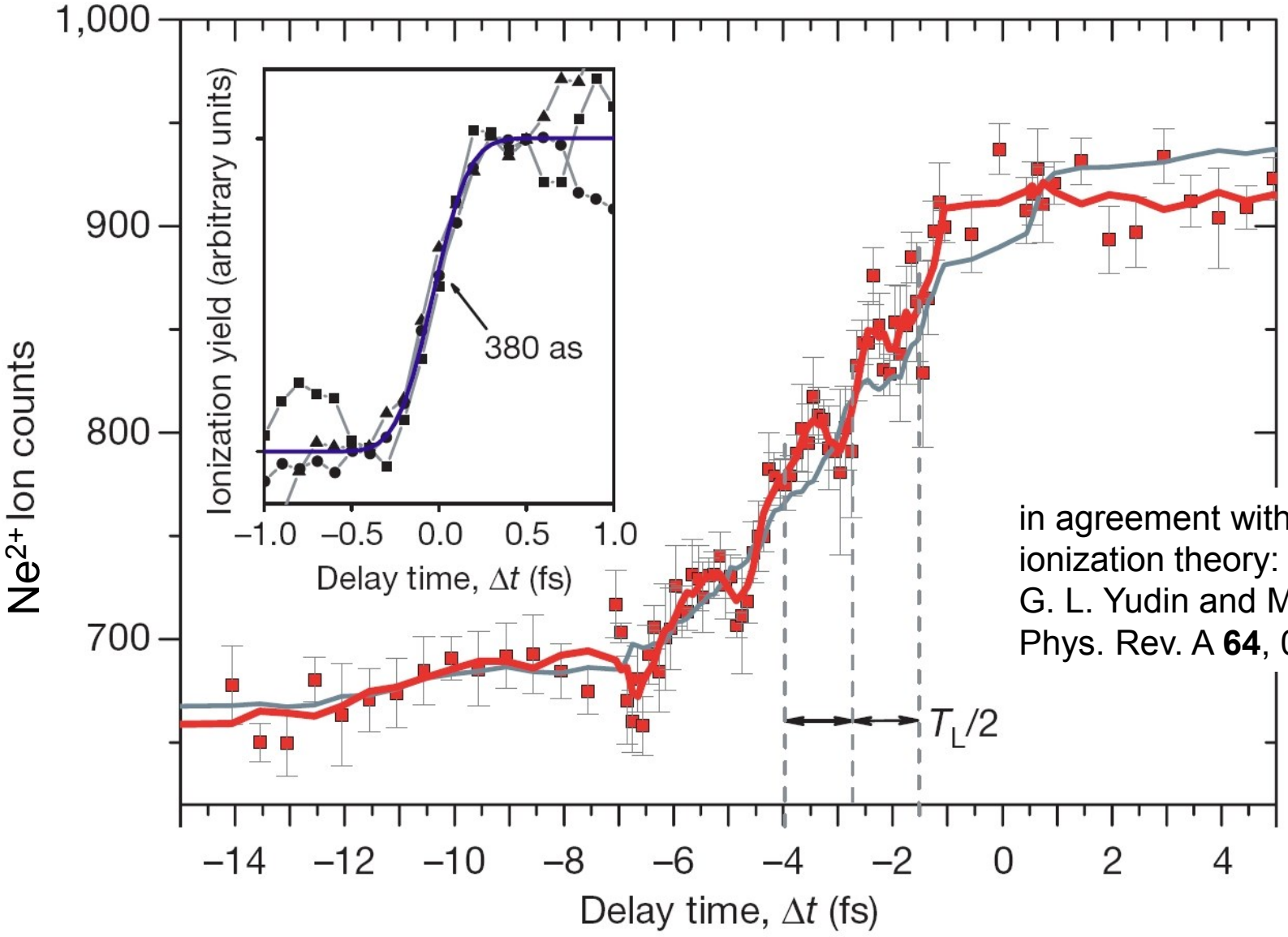

in agreement with tunnel ionization theory:
G. L. Yudin and M. Y. Ivanov, Phys. Rev. A **64**, 013409 (2001)

M. Uiberacker *et al.*, Nature **446**, 627 (2007)

12.3.9 Attoscience beamline at MPQ Garching

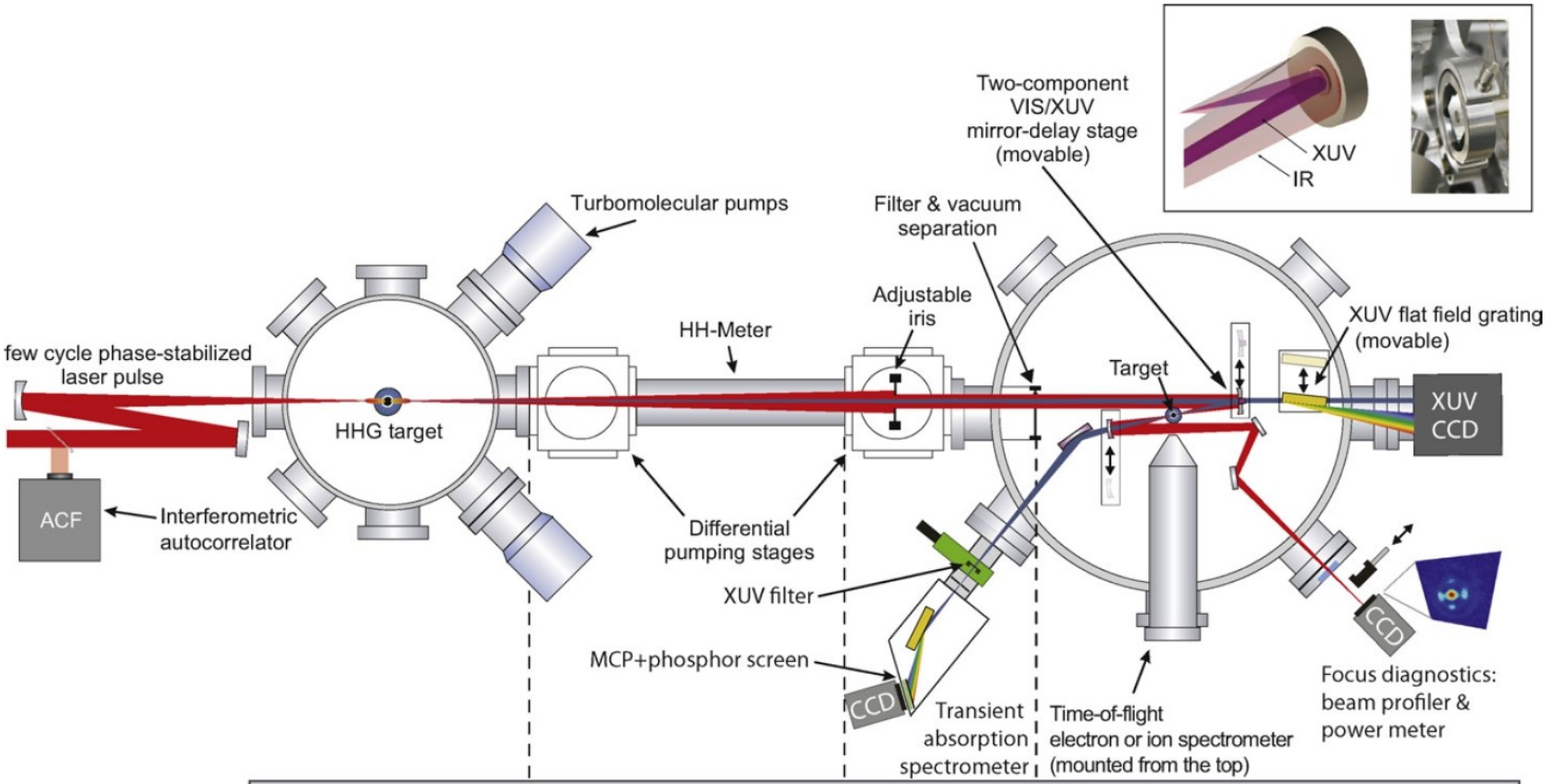

M. Schultze *et al.*, J. Electron Spectrosc. Relat. Phenom. **184**, 68 (2011)

12.3.9 Attoscience beamline at ETH Zürich

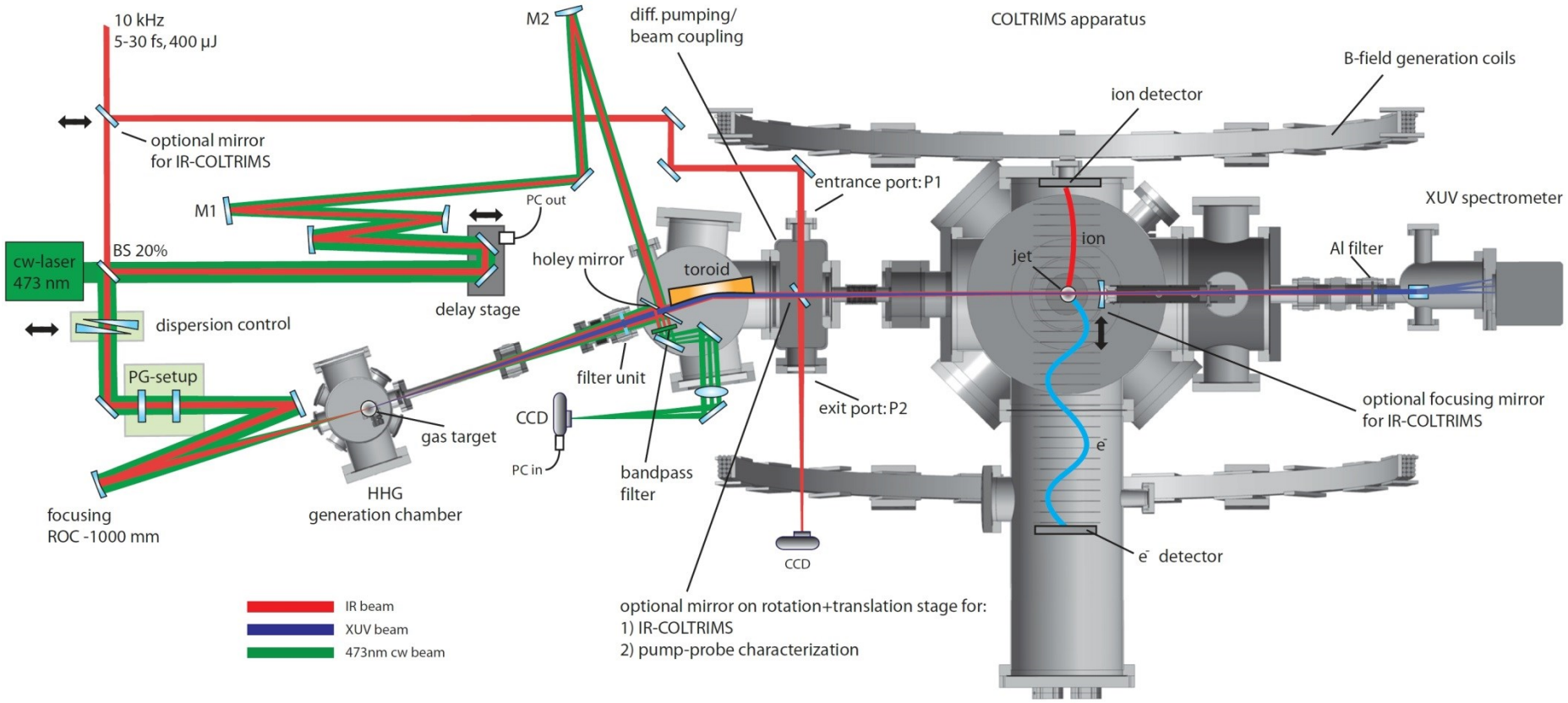

M. Sabbar *et al.*, Rev. Sci. Instrum. **85**, 103113 (2014)